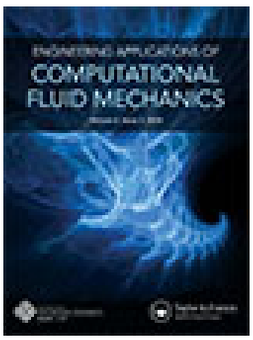

Engineering Applications of Computational Fluid Mechanics

ISSN: 1994-2060 (Print) 1997-003X (Online) Journal homepage: https://www.tandfonline.com/loi/tcfm20

A Fine Grid Solution for a Lid-Driven Cavity Flow Using Multigrid Method

D. Santhosh Kumar, K. Suresh Kumar & Manab Kumar Das

To cite this article: D. Santhosh Kumar, K. Suresh Kumar & Manab Kumar Das (2009) A Fine Grid Solution for a Lid-Driven Cavity Flow Using Multigrid Method, Engineering Applications of Computational Fluid Mechanics, 3:3, 336-354, DOI: 10.1080/19942060.2009.11015275

To link to this article: https://doi.org/10.1080/19942060.2009.11015275

Engineering Applications of Computational Fluid Mechanics Vol. 3, No. 3, pp. 336–354 (2009)

A FINE GRID SOLUTION FOR A LID-DRIVEN CAVITY FLOW USING MULTIGRID METHOD

D. Santhosh Kumar*, K. Suresh Kumar* and Manab Kumar Das**

** Department of Mechanical Engineering, Indian Institute of Technology Guwahati, North Guwahati, Guwahati – 781039, Assam, India*
*** Department of Mechanical Engineering, Indian Institute of Technology Kharagpur, Kharagpur, West Bengal, 721302, India.*
E-Mail: manab@mech.iitkgp.ernet.in (*Corresponding Author*)

ABSTRACT: This article presents the numerical solution of two dimensional fluid flow problem using multigrid method (MGM) full approximation scheme (FAS). Laminar flow in a square cavity with a moving wall is calculated for different Reynolds number on a fine uniform grid of 513×513. The finite volume method through the concepts of colocated grid and SIMPLEC algorithm has been applied. The method is fully conservative and uses higher order schemes (QUICK scheme) for convective fluxes and second order central differencing for diffusion fluxes. The numerical solutions of 2D incompressible flow in a driven cavity are presented. The multigrid implementation is documented in detail. The steady driven cavity solutions are computed for $Re \leq 10000$ with maximum absolute residual less than 10^{-8}. Detailed results are presented and the percentage deviation of midplane velocity from the established results is also calculated.

Keywords: fine grid, multigrid, driven cavity flow, FAS

1. INTRODUCTION

The lid-driven cavity flow problem has been investigated by many researchers because it contains a rich fluid flow physics manifested by boundary layer on the wall and multiple counter-rotating recirculation regions in the corners of the cavity based upon the Reynolds number (*Re*). Even though it is solved by many researchers, their results deviate from each other for $\mathrm{Re} \geq 1000$. These deviations are due to the type of discretization scheme, number of cells and method of solving used. In order to achieve an accurate solution, a very fine grid combined with higher order discretization scheme using SIMPLEC method is applied, for which a single-grid method exhibits a poor convergence behavior. Multigrid methods are more suitable for such system because of their ability to give grid independent convergence rates as the number of grid points is increased to large values in a fixed domain.

There are two broad categories of multigrid method: correction schemes (CS) and full approximation schemes (FAS). The correction scheme is applicable to linear systems only. It operates with corrections to the solution on coarse grids, which are eventually added to the absolute fine-grid solution. A full approximation scheme solves non-linear equations for approximations to the solution rather than for correction schemes. Sivaloganathan and Shaw (1988) adopted the full approximation multigrid method and achieved a large reduction in CPU time. They used a staggered grid arrangement, in which grid-coarsening process was difficult because of the use of three different sets of cells. Hence a colocated grid layout (Rhie and Chow, 1983) to eliminate pressure wiggles is used in the present work. Discussion of the relative merits between the two types of grid layout can be found in Peric, Kessler and Scheuerer (1998). Hortmann and Peric (1990) and Lien and Leschziner (1994) used full approximation scheme with colocated finite volume method and showed a dramatic accelerations in convergence over a single-grid method. A few researchers (Sathyamurthy and Patankar, 1994; Karki, Sathyamurthy and Patankar, 1996; Lilek, Muzaferija and Peric, 1997; Cornelius, Volgmann and Stoff, 1999) have carried out simulations of the cubical cavity flow using multigrid method The available results indicate that multigrid based solution procedure requires less computing time compared to single-grid method. In the present work, the algorithm of FAS multigrid method is documented and using this method a fine-grid solution for a lid-driven cavity problem is obtained. The main purpose is to gather extensive numerical results for $\mathrm{Re} \leq 10000$, hoping that these results could serve

Received: 29 Oct. 2008; Revised: 2 Jan. 2009; Accepted: 4 Feb. 2009

as benchmark. The study has been conducted for a range of Reynolds numbers, and quantitative comparisons with the results available from the published literature are drawn.

2. NUMERICAL METHODS

The present problem of lid-driven in a square-cavity is numerically solved using the full approximation storage multigrid method. The governing equations are discretized on a co-located grid arrangement using the finite volume method. The Quadratic Upwind Interpolation for Convective Kinematics (QUICK) scheme is employed for the convective terms in the momentum equations. The convergence criterion used here requires that the mass residual should be less than 10^{-8}. The nondimensional equations governing the conservation of mass and momentum can be written as follows:

$$\frac{\partial u}{\partial x}+\frac{\partial v}{\partial y}=0 \tag{1}$$

$$\frac{\partial (u^2)}{\partial x}+\frac{\partial (uv)}{\partial y}=-\frac{\partial p}{\partial x}+\frac{1}{Re}\left(\frac{\partial^2 u}{\partial x^2}+\frac{\partial^2 u}{\partial y^2}\right) \tag{2}$$

$$\frac{\partial (uv)}{\partial x}+\frac{\partial (v^2)}{\partial y}=-\frac{\partial p}{\partial y}+\frac{1}{Re}\left(\frac{\partial^2 v}{\partial x^2}+\frac{\partial^2 v}{\partial y^2}\right) \tag{3}$$

Therefore, the general equation can be written as

$$\frac{\partial (u\phi)}{\partial x}+\frac{\partial (v\phi)}{\partial y}=-\frac{\partial}{\partial x}\left(\Gamma^{\phi}\frac{\partial \phi}{\partial x}\right)+\frac{\partial}{\partial yx}\left(\Gamma^{\phi}\frac{\partial \phi}{\partial y}\right)+S^{\phi} \tag{4}$$

where ϕ = dependent variable, Γ^{ϕ} = diffusion coefficient and S = source term.

In Eq. (4), terms on the left represent the net convection flow. The two terms on the right represent the net diffusion and the last term the source generation. The mass conservation is obtained by setting

$$\phi = 1,\ \Gamma^{\phi} = 0,\ S = 0$$

Similarly, the momentum equation in the x direction is obtained when

$$\phi = u,\quad \Gamma^{\phi} = \frac{1}{Re},\quad S^{\phi} = -\frac{\partial p}{\partial x}$$

2.1 Discretization method

The flow governing equations are discretized based on finite volume co-located method. In this method the calculation domain is divided into a number of non-overlapping control volumes such that there is one control volume surrounding each grid point. The differential equation is integrated over each control volume yielding a discretised equation at each nodal point. The convective fluxes at the interface are computed by using the QUICK scheme and central differences for the diffusive cell-face fluxes. The QUICK scheme was first given by Leonard (1979). It uses the quadratic interpolation between two upstream neighbours and one down stream neighbour in order to evaluate the value of ϕ at the control volume interface. The value of ϕ at the east face of the control volume (see Fig. 1) is given by the quadratic interpolation.

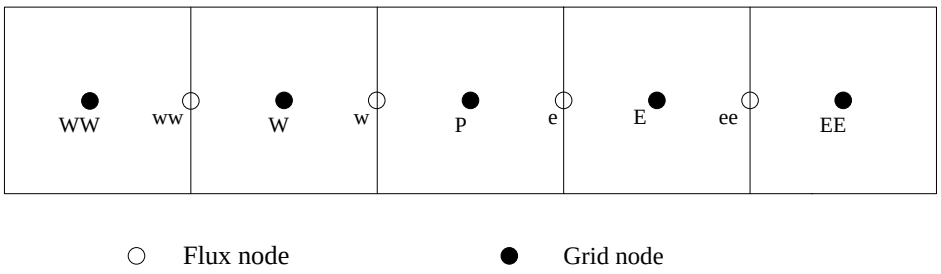

Fig. 1 Schematic diagram for interpolation formulae for the uniform colocated grid.

$$\phi_e = \frac{3}{8}\phi_E + \frac{3}{4}\phi_P - \frac{1}{8}\phi_W \qquad if \quad F_e > 0 \tag{5}$$

$$\phi_e = \frac{3}{8}\phi_P + \frac{3}{4}\phi_E - \frac{1}{8}\phi_E E \qquad if \quad F_e > 0 \tag{6}$$

Therefore the convective flux term can be summarized as

$$F_e\phi_e = \left(\frac{3}{8}\phi_E + \frac{3}{4}\phi_P - \frac{1}{8}\phi_W\right)\left[|0, F_e|\right] - \left(\frac{3}{8}\phi_P + \frac{3}{4}\phi_E - \frac{1}{8}\phi_{EE}\right)\left[|0, -F_e|\right] \tag{7}$$

where the operator $[|x, y|]$ denotes the maximum of the two arguments x and y and $Fe > 0$ implies that the flow is in the positive x-direction. The variable Fe is called the strength of convection and is given by $Fe = u\Delta y$. The deferred QUICK scheme (Hayase, Humphrey and Greif, 1992) which uses a first order upwind scheme with third order correction is applied in the present work. The deferred QUICK scheme is written as shown in the equation below where superscript n represents the latest value of the variable and n-1 represents the value of the variable in the previous iteration.

$$F_e \phi_e = \left(\phi_p^n + \frac{1}{8}\left(3\phi_E - 2\phi_P - \phi_W\right)^{n-1} \right) - \left[|0, F_e|\right] - \left(\phi_p^n + \frac{1}{8}\left(3\phi_P - 2\phi_E - \phi_{EE}\right)^{n-1} \right) - \left[|0, F_e|\right] \quad (8)$$

The QUICK scheme is not applicable to the nearest boundary points because some points cross the physical domain. So to the nearest boundary points, central difference scheme is used for calculating the variable ϕ.

3. DESCRIPTION OF MULTIGRID ALGORITHM

The multigrid method is one of the most efficient general iterative methods. Unlike other iterative methods, multigrid algorithms order convergence rates that are independent of the number of grid points. The multigrid method adopted in this work is the Full Approximation Scheme (FAS) which has been described in detail in literature (Sivaloganathan and Shaw, 1988; Lien and Leschziner, 1994) and hence the present description of the multigrid FAS process will be brief. The flow governing equations are discretized based on the finite volume colocated method. The convection fluxes at the interface are computed by using the QUICK scheme and central differences for diffusive cell-face fluxes, leading to a weighted average formula of the form

$$A_p \phi_p = \sum_{nb} A_{nb} \phi_{nb} + S_\phi \quad (9)$$

where nb denotes neighbours of the node P involved in the interpolation polynomials, and ϕ stands for momentum components. To solve the coupled system, a SIMPLEC algorithm (Doormaal and Raithby, 1984), modified in such a manner so as to implicitly account for the effects of the anisotropic coefficients, is used as a smoothing scheme for multigrid method. The present multigrid method, applied to a two-grid system, commences by performing a few finite volume iterations using the SIMPLEC algorithm on the finest grid having a mesh size h. The same procedure of colocated finite volume method is followed on the fine grid. Then, the unconverged momentum equations having residuals R_u and R_v can be expressed as

$$A_p^* u_p^* = \sum_{nb} A^*_{nb} u^*_{nb} + S_u^* + \left(p_P^* - p_E^*\right) A_e + R_u \quad (10)$$

$$A_p^* v_p^* = \sum_{nb} A^*_{nb} v^*_{nb} + S_v^* + \left(p_P^* - p_N^*\right) A_e + R_v \quad (11)$$

In order to obtain the converged solutions, the corrections for velocity components and pressure are introduced, namely

$$u = u^* + u', \quad p = p^* + p' \quad (12)$$

so that residual R_u vanishes,

$$A_p u_p = \sum_{nb} A_{nb} u_{nb} + S_u + \left(p_P - p_E\right) A_e \quad (13)$$

Subtracting Eq. (10) from Eq. (13) yields

$$A_P u_P - A_P^* u_P^* = \sum_{nb} A_{nb} u_{nb} - \sum_{nb} A^*_{nb} u^*_{nb} + S_u - S_u^* + (p_P - p_E - p_P^* + p_E^*) A_e - R_u \quad (14)$$

The analogous equation for v arises as

$$A_P v_P - A_P^* v_P^* = \sum_{nb} A_{nb} v_{nb} - \sum_{nb} A^*_{nb} v^*_{nb} + S_v - S_v^* + (p_P - p_N - p_P^* + p_N^*) A_n - R_v \quad (15)$$

Eq. (14) and Eq. (15) serve as the basis for deriving the coarse-grid equation. Now assemble the above equations for u, v on the coarse grid whose solutions are $\hat{u}, \hat{v}$

$$A_p \hat{u}_p = \sum_{nb} A_{nb} \hat{u}_{nb} + \hat{S}_u + (p'_p - p'_E) A_e + A_p \hat{u}_p - \sum_{nb} A_{nb} \tilde{u}_{nb} - \tilde{S}_u - \tilde{R}_u \quad (16)$$

$$A_p \hat{v}_p = \sum_{nb} A_{nb} \hat{v}_{nb} + \hat{S}_v + (p'_p - p'_N) A_n + A_p \hat{v}_p - \sum_{nb} A_{nb} \hat{v}_{nb} - \tilde{S}_v - \tilde{R}_v \quad (17)$$

Eqs. (16) and (17) appear identical to Eq. (10) and (11); however, the equations now contain an additional source term. The variables and operators denoted by (^) are modified during the iteration on the coarser grid level. The vectors that have been transferred from fine grid level are denoted by (~) and are referred to as restricted quantities. The manner is which the variables are restricted will be explained in the next section. The underlined terms remain unchanged during the iteration on the coarser grid and appear as an extra source term in the above equation. The quantities with superscript (~) are used as initial guess for (^) quantities which are changed owing to the restricted residuals $\tilde{R}_u$ and $\tilde{R}_v$ when iterating the coarse grid. If the residual is zero, the solution will be $\hat{u} = \tilde{u}$, i.e., $\tilde{R}_u = 0$. It is noted that pressure correction equation is linear in pressure and therefore, no restriction of pressure from fine to coarse grid is needed. Now, the SIMPLEC smoothing scheme applied to the coarse grid equations is summarized. This sequence involves the following steps:

1. The initial state is:

$$\hat{u} = \tilde{u}, \quad \hat{v} = \tilde{v}, \quad p' = 0 \quad (18)$$

2. Perform a few iterations on the coarse-grid momentum equations.

3. The cell-face velocities are corrected by means of the following relations, applicable to the east and north faces of the volume cell, respectively:

$$u'_e = \hat{u}_e - \tilde{u}_e + \Delta V_e \overline{\left(\frac{1}{A_p}\right)}_e \left[\overline{\left(\frac{\partial p'}{\partial x}\right)}_e - \left(\frac{\partial p'}{\partial x}\right)_e \right] \quad (19)$$

$$v'_n = \hat{v}_n - \tilde{v}_n + \Delta V_n \overline{\left(\frac{1}{A_p}\right)}_n \left[\overline{\left(\frac{\partial p'}{\partial y}\right)}_n - \left(\frac{\partial p'}{\partial y}\right)_n \right] \quad (20)$$

The terms in the Eqs. (19) and (20) with over-bars are simply arithmetic averages of values of the nodes adjacent to the appropriate faces (P and E or P and N) and also they reflect the conventional Rhie and Chow (1983) interpolation strategy required to secure freedom from odd-even oscillations in a colocated framework. Analogous expressions for the west and south faces can be derived in a similar manner. The mass residuals of coarse grid based on these face velocities are calculated.

4. The face-velocity corrections (denoted by double primes) are derived from truncated versions of Eq. (19) and Eq. (20)

$$u''_e = a_e \left(\frac{1}{(A_p - \sum A_{nb})} \right)_e (p''_P - p''_E) \quad (21)$$

$$v''_n = a_n \left(\frac{1}{(A_p - \sum A_{nb})} \right)_n (p''_P - p''_N) \quad (22)$$

5. The coarse-grid pressure correction equation is derived by substituting the face velocity corrections into the mass-continuity constraint. The pressure correction equation is p'', given by

$$A_p p''_p = \sum_{nb} A_{nb} p''_{nb} + R'_{nb} \quad (23)$$

where R'_{nb} indicates the mass unbalance.

6. Eq. (23) is solved, and the related pressure and face velocity corrections are updated using correction equations (21) and (22).

7. The algorithm returns to step 2 to terminate one outer relaxation sweep.

After performing v_H relaxation sweeps with the initial quantities $\tilde{\phi}$, the coarse-grid solution is obtained. Therefore the coarse grid correction can be calculated by

$$[\delta\phi]^c = [\hat{\phi}] - [\tilde{\phi}] \quad (24)$$

If $\phi = p'$ (pressure correction), then

$$[\delta\phi]^c = [\hat{\phi}] \quad (25)$$

The coarse-grid corrections are interpolated back (prolongated) to the fine grid to adjust the fine-grid solutions. This is followed by v_h smoothing iterations designed to eliminate any high-

frequency error components introduced by the prolongation process.

$$[\delta\phi]^f = [I_c^f][\delta\phi]^c \tag{26}$$

and added to the previous intermediate approximations

$$[\phi]_{new}^f = [\phi]_{old}^f + \lambda[\delta\phi]^f \tag{27}$$

where λ is an under relaxation factor, $0 \le \lambda \le 1$. Since the updated solutions on the fine grid will still not, in general, be converged, it is necessary to repeat the above two-level cycle until full convergence is achieved.

3.1 Restriction

Transfer of variables from the fine-grid to the next level of the coarser-grid is termed restriction and the corresponding operator is denoted by I_f^c, with *f* and *c* denoting fine and coarse, respectively. In a cell centre finite volume algorithm no nodes on the fine-grid ever coincide with those of the coarse-grid whether staggered or colocated and therefore, the transfer of variables from the fine- to the coarse-grid has to be performed by interpolation. The transfer of residuals requires no interpolation because the coarse-grid balance equation is equal to the sum of the four balance equations for the corresponding fine-grid control volume. The arrangement of variables is shown in Fig. 2 and divided into three regions: a- inner region, b- west boundary and c- north-west corner. Thus the restriction operator can be expressed as

$$\tilde{\phi} = \phi^c = [I_f^c]\begin{bmatrix}\phi^1\\ \phi^2\\ \phi^3\\ \phi^4\end{bmatrix}^f \tag{28}$$

For example, for the inner region away from the boundaries,

$$[I_f^c] = \frac{1}{4}[1 \quad 1 \quad 1 \quad 1] \tag{29}$$

while for the west boundary,

$$[I_f^c] = \frac{1}{4}[2 \quad 2 \quad 0 \quad 0] \tag{30}$$

and for the north-west corner,

$$[I_f^c] = \frac{1}{4}[0 \quad 4 \quad 0 \quad 0] \tag{31}$$

The above equations represent bilinear interpolation formulae. The restriction operator pertaining to the residuals is

$$\tilde{R}_\phi = R_\phi^c = [I_f^c]\begin{bmatrix}R_\phi^1\\ R_\phi^2\\ R_\phi^3\\ R_\phi^4\end{bmatrix}^f \tag{32}$$

where $[I_f^c] = [1 \ 1 \ 1 \ 1]$.

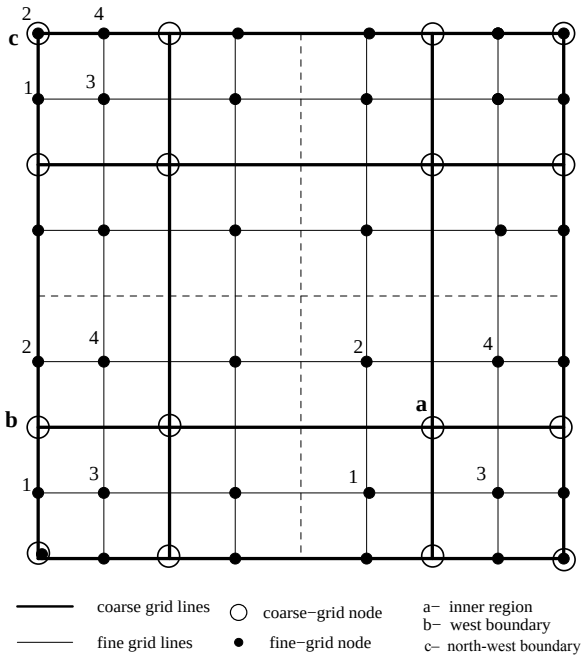

Fig. 2 Restriction of mass fluxes and variables.

3.2 Prolongation

The transfer of variables from the coarse- to the fine-grid level is termed prolongation and the corresponding operator is denoted by I_c^f, through which the corrections obtained from the coarse-grid solutions are passed to the finer-grid to update the solution on it. The 2D computational domain can be divided into three parts: A- the inner region, B- the boundary strips and C- the boundary corners (Fig. 3). The nature of the prolongation operator depends on the region under consideration and each region has its own prolongation operator and can be expressed as

$$\begin{bmatrix} \delta\phi^1 \\ \delta\phi^2 \\ \delta\phi^3 \\ \delta\phi^4 \end{bmatrix}^f = [\, I_c^f \,] \begin{bmatrix} \delta\phi^1 \\ \delta\phi^2 \\ \delta\phi^3 \\ \delta\phi^4 \end{bmatrix}^c \tag{33}$$

The prolongation operator I_c^f has the following forms:
For the inner region:

$$[\, I_c^f \,] = \frac{1}{16} \begin{bmatrix} 9 & 3 & 3 & 1 \\ 3 & 9 & 1 & 3 \\ 3 & 1 & 9 & 3 \\ 1 & 3 & 3 & 9 \end{bmatrix}, \tag{34}$$

for the west boundary:

$$[\, I_c^f \,] = \frac{1}{16} \begin{bmatrix} 0 & 0 & 6 & 2 \\ 0 & 0 & 2 & 6 \\ 3 & 1 & 3 & 1 \\ 1 & 3 & 1 & 3 \end{bmatrix}, \tag{35}$$

and for north-west corner:

$$[\, I_c^f \,] = \frac{1}{16} \begin{bmatrix} 0 & 0 & 2 & 2 \\ 0 & 0 & 0 & 4 \\ 1 & 1 & 1 & 1 \\ 0 & 2 & 0 & 2 \end{bmatrix} \tag{36}$$

Similar relations can be applied to the other boundaries and corners.

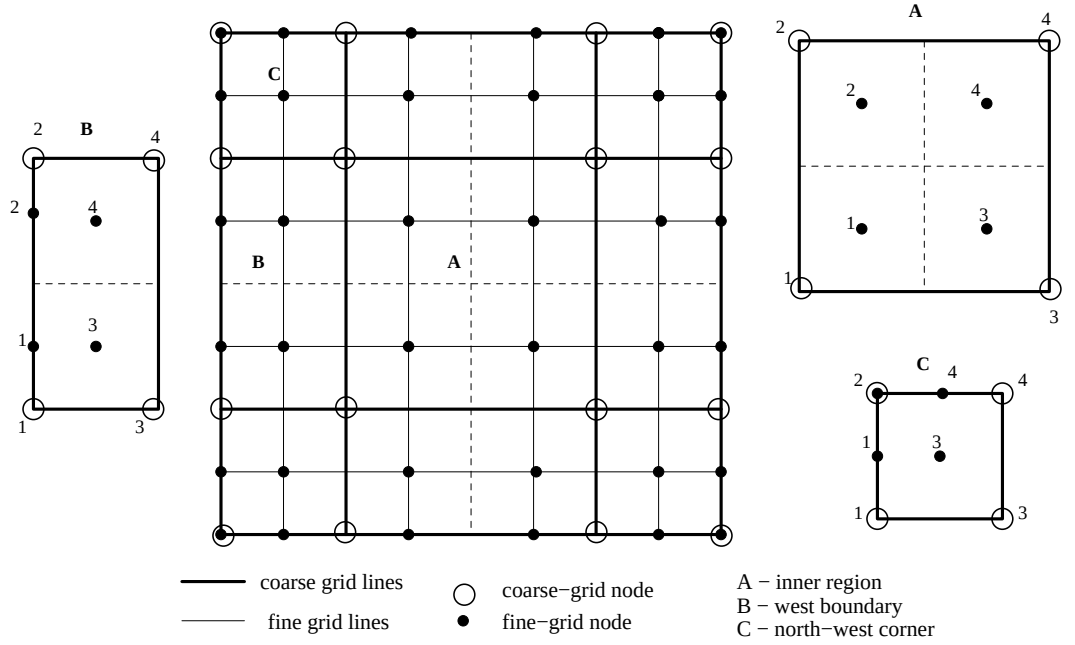

Fig. 3 Grid stencil for prolongation operator.

4. APPLICATION TO LID-DRIVEN CAVITY PROBLEM

The multigrid FAS algorithm described above has been implemented to solve the lid-driven cavity problem. The driven cavity is the prototypical recirculation flow and has long been used as a standard test problem for Navier-Stoke solvers. Flow is set up in a square cavity with three stationary walls and a top lid that moves to the right with constant speed ($u = 1$). The boundary condition and schematics of the vortices generated in a driven cavity flow are shown in Fig. 4. The letters T, B, L and R denote the top, bottom, left and right of the cavity, and the numbers denote the hierarchy of secondary vortices appear in the flow. There are many numerical methods applied to this problem which yield same result for $Re \leq 1000$; however, the results start to deviate from each other for higher *Re* (Hou et al., 1995). This is an incentive to study this problem and attempt to give some illuminative results. The test problem has been solved using the FAS multigrid method with the SIMPLEC algorithm as a smoother, and TDMA solver over a range of Reynolds number from 1000 to 10000. The results have been compared with well established results (Ghia, Ghia and Shin,

1982; Erturk, Corke and Gokcol, 2005; Botella and Peyret, 1998). To test the grid independence of the solution, numerical experiments were performed for three uniform fine grids of 129×129, 257×257 and 513×513 for $Re = 1000$. The centre line u-velocity ($x = 0.5$) is tabulated in Table 1 and shows that an equally spaced grid of 513×513 is quite good. Refining the grid further would produce the same results.

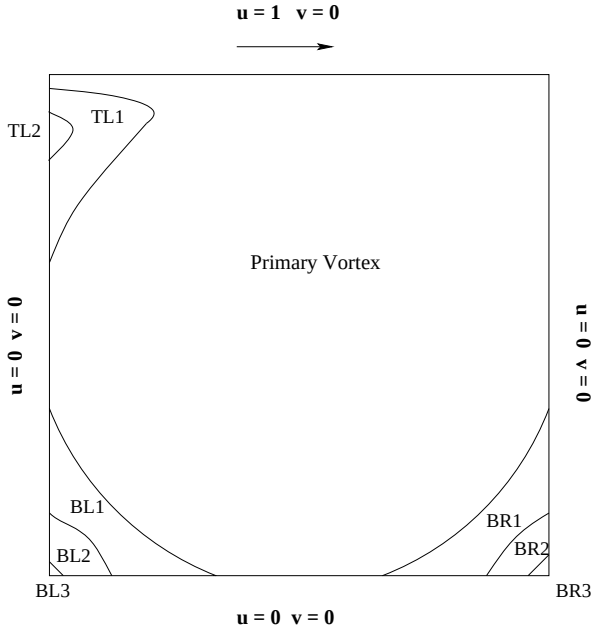

Fig. 4 Schematic view of lid-driven cavity flow.

Table 1 Grid independence test of centreline u-velocity for various grid sizes.

y	129×129	257×257	513×513
0.9688	0.5785	0.5803	0.5807
0.9531	0.4697	0.4716	0.4722
0.7344	0.1868	0.1881	0.1886
0.5	-0.0620	-0.0620	-0.0620
0.2813	-0.2791	-0.2800	-0.2802
0.1016	-0.2948	-0.299	-0.3001
0.0625	-0.1981	-0.2012	-0.202

5. RESULTS AND DISCUSSIONS

Streamline contours for various Reynolds numbers on 513×513 grids are shown in Fig. 5 through 7. These streamline patterns exhibit the formation of counter-rotating secondary vortices which appears as the Reynolds number increases. A magnified view of the various secondary vortices is also included. An interesting point is that a tertiary vortex is clearly visible for $Re = 1000$ (see Fig. 5), indeed, on coarse grids (129×129 grids) there is no appearance of this vortex at the bottom right and bottom left corners of the cavity. This shows that finer grids would resolve the corner vortices better. The augmentation of these tertiary vortices with increase in Reynolds number is also shown in Figs. 6 and 7. Figure 8 clearly shows the thinning of the wall boundary layers with increase in Re, although the rate of this thinning is very slow for $Re \geq 5000$. From these profiles, it is seen that changes in u and v velocities are almost linear in the core of a primary vortex as Re increases. This would indicate that in this region the vorticity is uniform.

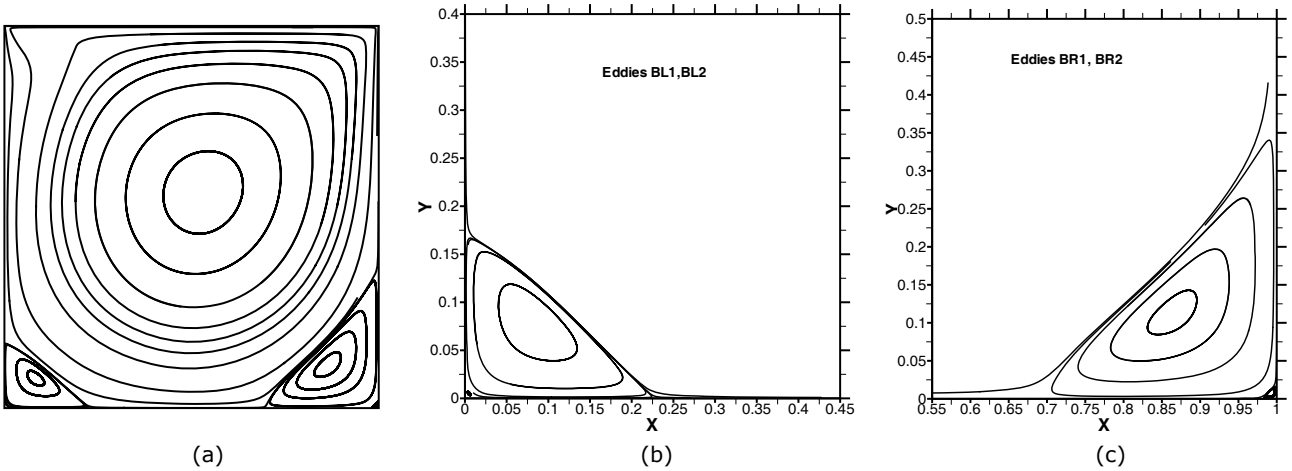

Fig. 5 Streamline contours of primary and secondary vortices for $Re = 1000$.

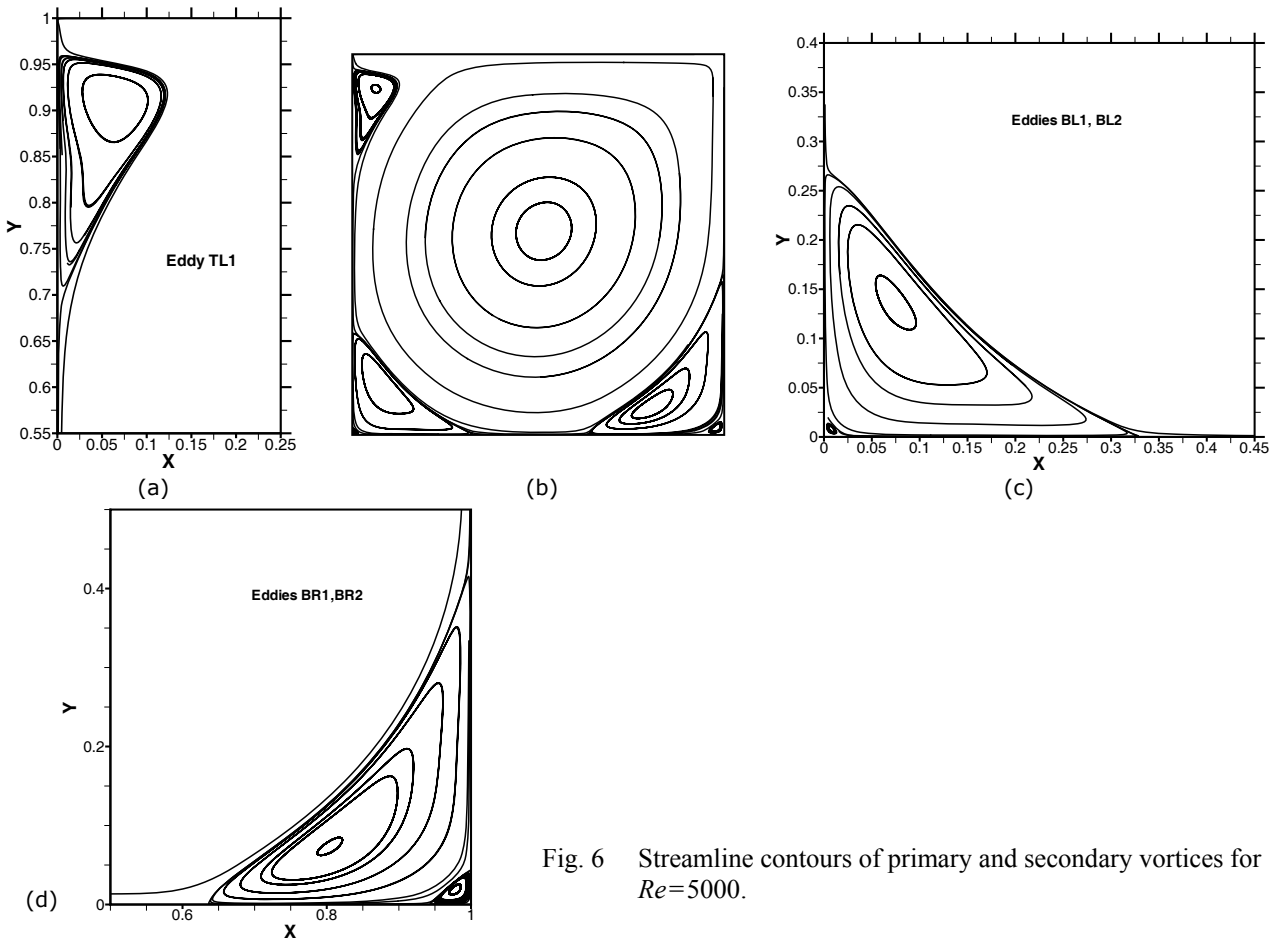

Fig. 6 Streamline contours of primary and secondary vortices for Re=5000.

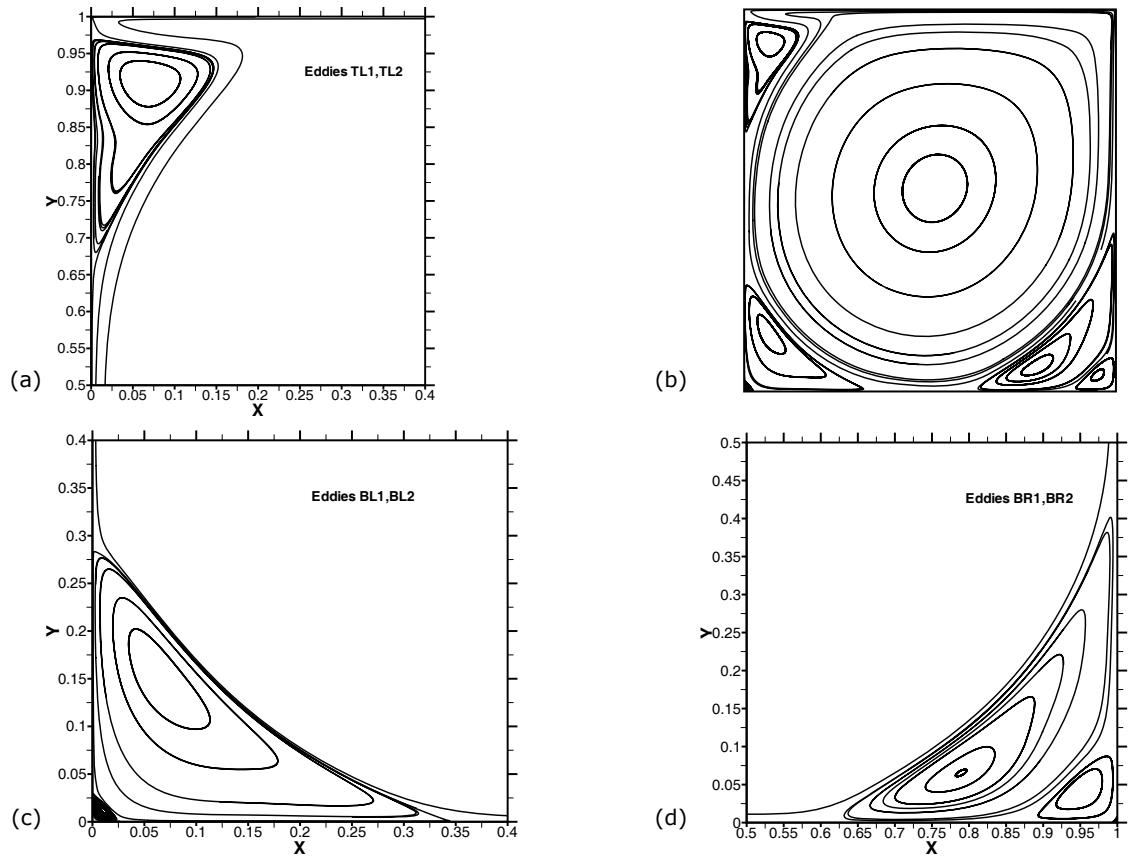

Fig. 7 Streamline contours of primary and secondary vortices for Re=7500.

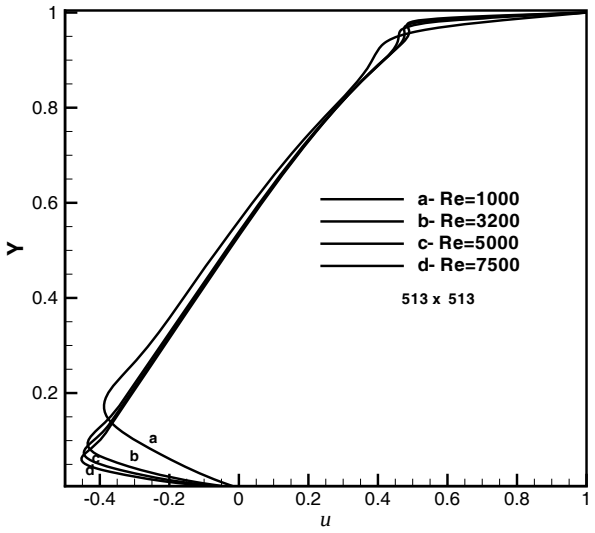

Fig. 8 Centreline *u*-velocity for various Reynolds numbers.

Fig. 9 shows the *u* velocity profiles along a vertical line and Fig. 10 represents the *v* velocity profiles along a horizontal line passing through the geometric centre of the cavity. These profiles shows that the results are in good agreement with those of Erturk, Corke and Gokcol (2005) but have a small discrepancy with Ghia, Ghia and Shin (1982) for $Re = 5000$ and 7500. Tables 2–5 summarizes the percentage deviations of centerline velocity values from the corresponding results available in the literature. It comes out clearly from the tables that the computed values for all Reynolds numbers show less than 1% deviation from those of Erturk, Corke and Gokcol (2005) produced on 601×601 grids, but has large deviation from those of Ghia, Ghia and Shin (1982) produced on 129×129 grids. Botella and Peyret (1998) have tabulated highly accurate Chebyshev collocation spectral velocity data along a vertical line and along a horizontal line passing through the geometric centre of the cavity for $Re = 1000$. In comparison with Botella and Peyret (1998), the present solution shows a remarkable agreement between the two solutions with a maximum difference of 0.19 percent, as seen in Tables 6 and 7. In view of the above remarks, the present result is in good agreement with the findings of Erturk, Corke and Gokcol (2005) and Botella and Peyret (1998). Ghia, Ghia and Shin (1982) have used a grid size of 129×129 with second order accuracy. This may be the reason for the deviation from the present solution. Therefore, the result obtained by Ghia, Ghia and Shin (1982) is an under resolved solution. Most recently Bruneau and Saad (2006) revisited the lid-driven cavity flow problem which was a continued study of Bruneau and Jouron (1990) and have given a detailed investigation of Hopf bifurcation obtained at Reynolds numbers close to $Re = 8000$ using a very fine grid of 2048×2048. When comparing the *u*-velocity given in Table 8, the present results are coherent with the results in Bruneau and Saad (2006). For all these results until $Re = 7500$, the grid convergence is achieved to a tolerance of 10^{-8}. At $Re = 10{,}000$, there is no convergence of the residual below 10^{-3} (see Fig. 11) and the residual history shows that the solution is periodic in nature. Initially there is a small tertiary vortex at the bottom left corner at $Re = 5000$, and this eddy grows in size up to $Re = 7500$. Also a quaternary vortex begins to appear in the bottom right corner at this Reynolds number. From this it is conjectured that these eddies play a significant role to make the flow unstable. Many studies (Bruneau and Jouron, 1990; Fortin et al., 1997; Poliashenko and Aidun, 1995; Hou et al., 1995; Auteri, Parolini and Quartapelle, 2002; Peng, Shiau and Hwang, 2003; Bruneau and Saad, 2006) predicted that Hopf bifurcation takes place between $Re = 7000$ and 9000. Figures 12(a) and 12(b) show the streamline contours for $Re = 10000$ at two different iteration levels. The former figure shows the growth of tertiary vortices at the bottom left corner after 20000 iterations and it seems that a steady solution will soon be reached. But later in the next 20000 iterations an interesting phenomenon of the emanation of new eddies at the top left corner is clearly seen in Fig. 12(b). The secondary vortices slightly deform the primary vortex, indeed, the primary vortex is still attached to the three walls of the cavity but the secondary vortices in the bottom left corner are unstable. Finally the left bottom secondary vortices split into two pieces (see Fig. 12(b)) where the primary vortex still remains stable. Therefore the velocity distribution in the primary vortex is fairly linear and hence the centreline velocities are in accordance with the results found in Ghia, Ghia and Shin (1982) and Erturk, Corke and Gokcol (2005) (see Fig. 13).

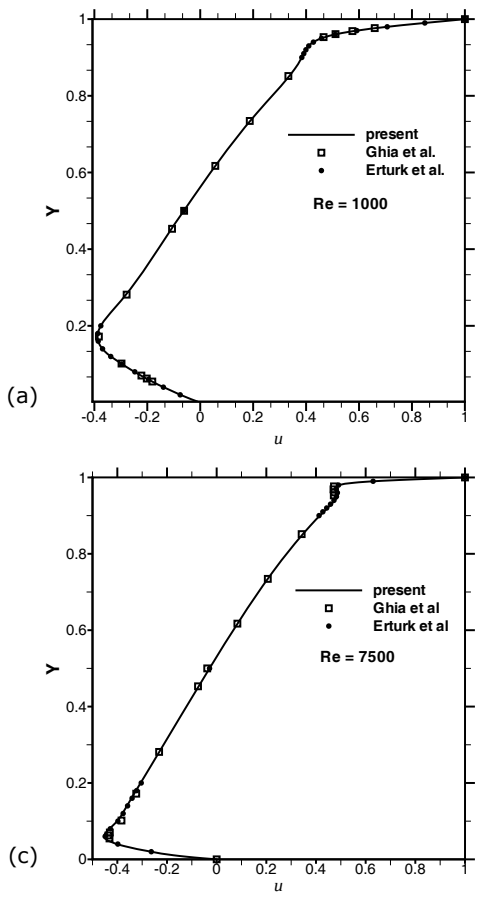

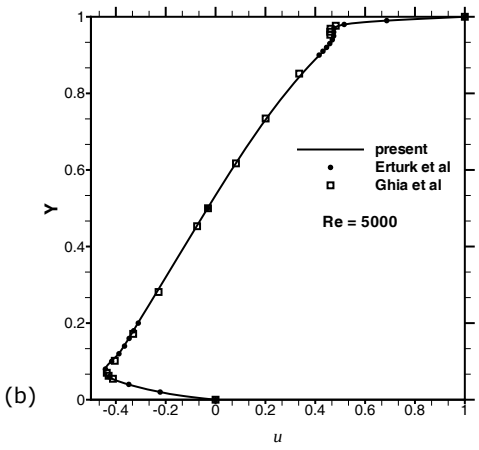

Fig. 9 *u*-velocity profile along vertical line passing through geometric centre at various Reynolds number.

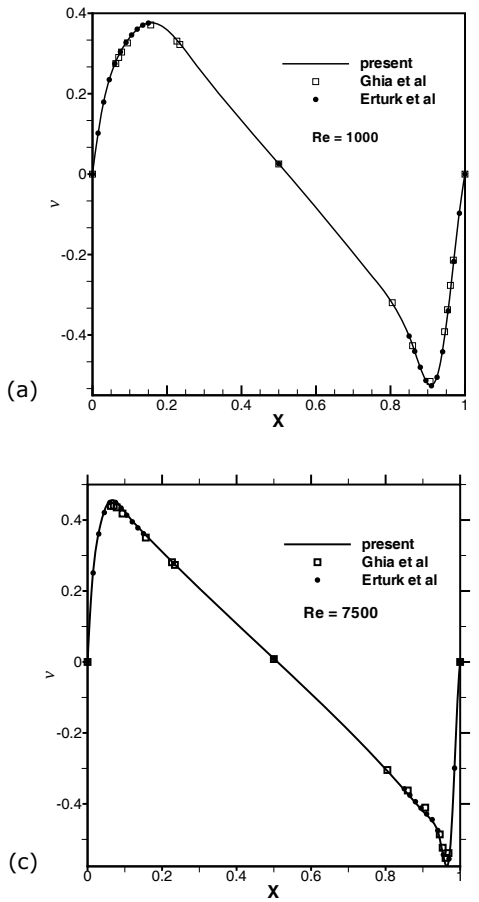

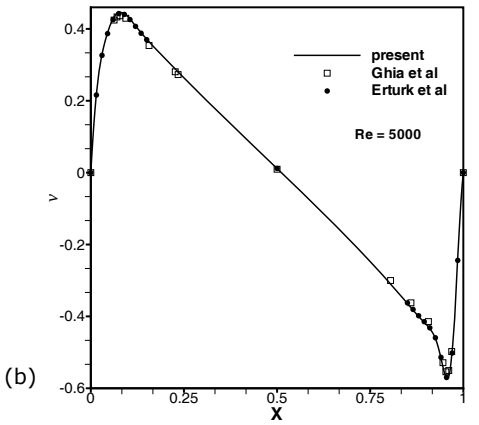

Fig. 10 *v*-velocity profiles along horizontal line passing through geometric centre at various Reynolds number.

Table 2 Percentage difference of centreline *u*-velocity with Ghia, Ghia & Shin (1982).

y	Re	1000	5000	7500	10000
	Ghia et al.	0.65928	0.48223	0.47244	0.47221
0.9766	present	0.66428	0.49601	0.48677	0.49115
	deviation	0.7586	2.85673	3.03277	4.0105
	Ghia et al.	0.57492	0.4612	0.47048	0.47783
0.9688	present	0.58069	0.47696	0.48693	0.49678
	deviation	1.0036	3.41782	3.49622	3.96501
	Ghia et al.	0.51117	0.45992	0.47323	0.4807
0.9609	present	0.51678	0.47649	0.49023	0.49784
	deviation	1.0971	3.60345	3.59191	3.56501
	Ghia et al.	0.46604	0.46036	0.47167	0.47804
0.9531	present	0.47217	0.47699	0.48853	0.49268
	deviation	1.3158	3.61304	3.57432	3.06292
	Ghia et al.	0.33304	0.33556	0.34228	0.34635
0.8516	present	0.337	0.34748	0.34728	0.34653
	deviation	1.189	3.55197	1.45933	0.05313
	Ghia et al.	0.05702	0.08183	0.08342	0.08344
0.6172	present	0.05696	0.08098	0.08355	0.08511
	deviation	-0.1001	-1.03825	0.15955	1.9994
	Ghia et al.	-0.0608	-0.03039	-0.038	-0.03111
0.5	present	-0.06205	-0.03208	-0.02894	-0.02726
	deviation	2.0584	5.57321	-23.84158	-12.36998
	Ghia et al.	-0.10648	-0.07404	-0.07503	-0.0754
0.4531	present	-0.10817	-0.07604	-0.0727	-0.071
	deviation	1.589	2.703	-3.10649	-5.83355
	Ghia et al.	-0.27805	-0.22855	-0.23176	-0.23186
0.2813	present	-0.28028	-0.23558	-0.23121	-0.22915
	deviation	0.8035	3.07723	-0.23602	-1.16967
	Ghia et al.	-0.38289	-0.3305	-0.32393	-0.32709
0.1719	present	-0.38829	-0.33743	-0.33215	-0.32885
	deviation	1.4098	2.09713	2.53759	0.53869
	Ghia et al.	-0.2973	-0.40435	-0.38324	-0.38
0.1016	present	-0.30011	-0.41598	-0.39852	-0.39115
	deviation	0.9465	2.87672	3.98654	2.93421
	Ghia et al.	-0.2222	-0.43643	-0.43025	-0.41657
0.0703	present	-0.22262	-0.44444	-0.44609	-0.39115
	deviation	0.1877	1.83466	3.68065	-6.10222
	Ghia et al.	-0.20196	-0.42901	-0.4359	-0.42537
0.0625	present	-0.20207	-0.43485	-0.45236	-0.44541
	deviation	0.055	1.36197	3.7761	4.71119
	Ghia et al.	-0.18109	-0.41165	-0.43154	-0.42735
0.0547	present	-0.18105	-0.41478	-0.44845	-0.453
	deviation	-0.0221	0.75963	3.91852	6.00211

Table 3 Percentage difference of centerline *v*-velocity with Ghia, Ghia & Shin (1982).

x	Re	1000	5000	7500	10000
	Ghia et al.	-0.21388	-0.49774	-0.53858	-0.54302
0.9688	present	-0.22759	-0.5174	-0.56579	-0.5761
	deviation	6.41107	3.94885	5.05292	6.09094
	Ghia et al.	-0.27669	-0.55069	-0.55216	-0.52987
0.9609	present	-0.2933	-0.56888	-0.57148	-0.54948
	deviation	6.00166	3.3024	3.49862	3.70072
	Ghia et al.	-0.33714	-0.55408	-0.52347	-0.49099
0.9531	present	-0.35489	-0.56835	-0.53663	-0.50586
	deviation	5.26339	2.57562	2.51476	3.02756
	Ghia et al.	-0.5155	-0.41442	-0.4105	-0.41496
0.9063	present	-0.52602	-0.42919	-0.42768	-0.42561
	deviation	2.04035	3.56305	4.18538	2.56555
	Ghia et al.	-0.31966	-0.30018	-0.30448	-0.30719
0.8047	present	-0.32008	-0.30968	-0.30706	-0.30557
	deviation	0.13233	3.16577	0.84636	-0.52801
	Ghia et al.	0.02526	0.00945	0.00824	0.00831
0.5	present	0.02578	0.01163	0.00971	0.00861
	deviation	2.0772	23.01587	17.87913	3.55884
	Ghia et al.	0.32235	0.2728	0.27348	0.27224
0.2344	present	0.32519	0.28036	0.27483	0.27157
	deviation	0.8801	2.76979	0.49473	-0.24647
	Ghia et al.	0.33075	0.28066	0.28117	0.28003
0.2266	present	0.33381	0.28859	0.28293	0.27953
	deviation	0.92517	2.82691	0.62596	-0.17927
	Ghia et al.	0.37095	0.35368	0.3506	0.3507
0.1563	present	0.37665	0.36438	0.35748	0.35249
	deviation	1.53552	3.02533	1.96321	0.51155
	Ghia et al.	0.30353	0.43648	0.43564	0.43124
0.0781	present	0.30965	0.44599	0.45062	0.44361
	deviation	2.0166	2.17971	3.43747	2.86847
	Ghia et al.	0.29012	0.43329	0.4403	0.43733
0.0703	present	0.29602	0.44231	0.45568	0.45337
	deviation	2.03295	2.08221	3.49398	3.66771
	Ghia et al.	0.27485	0.42447	0.43979	0.43983
0.0625	present	0.28046	0.43287	0.45529	0.45993
	deviation	2.04111	1.97847	3.52464	4.56927

Table 4 Percentage difference of centerline *u*-velocity with Erturk, Corke & Gokcol (2005).

y	Re	1000	5000	7500	10000
	Erturk et al.	0.8486	0.6866	0.63	0.5891
0.99	present	0.84884	0.6895	0.63519	0.59913
	deviation	0.0288	0.423	0.8232	1.70243
	Erturk et al.	0.7065	0.5159	0.4907	0.4837
0.98	present	0.70685	0.51936	0.49591	0.49242
	deviation	0.05	0.6697	1.0613	1.80174
	Erturk et al.	0.4582	0.4738	0.4824	0.4843
0.95	present	0.45868	0.4779	0.48654	0.48937
	deviation	0.1037	0.8643	0.8582	1.0477
	Erturk et al.	0.4276	0.4683	0.4723	0.4711
0.94	present	0.42804	0.47074	0.47622	0.47564
	deviation	0.1036	0.5208	0.8298	0.96307
	Erturk et al.	0.3913	0.4307	0.4275	0.4243
0.91	present	0.39163	0.43279	0.43095	0.42828
	deviation	0.0833	0.4846	0.8061	0.93849
	Erturk et al.	0.3838	0.4155	0.4123	0.4095
0.9	present	0.38408	0.41755	0.41556	0.41339
	deviation	0.074	0.4941	0.7909	0.94872
	Erturk et al.	-0.062	-0.0319	-0.0287	-0.0268
0.5	present	-0.06205	-0.03208	-0.02894	-0.02726
	deviation	0.0831	0.5759	0.8369	1.72276
	Erturk et al.	-0.3756	-0.31	-0.3038	-0.2998
0.2	present	-0.37581	-0.31144	-0.30613	-0.30332
	deviation	0.0562	0.4645	0.7653	1.17312
	Erturk et al.	-0.3869	-0.3285	-0.3222	-0.3179
0.18	present	-0.38713	-0.33001	-0.32464	-0.32149
	deviation	0.0592	0.4588	0.757	1.12929
	Erturk et al.	-0.369	-0.3652	-0.3587	-0.3543
0.14	present	-0.36941	-0.36687	-0.36141	-0.35782
	deviation	0.1111	0.4584	0.7558	0.99407
	Erturk et al.	-0.296	-0.4168	-0.3978	-0.3899
0.1	present	-0.29644	-0.4185	-0.40051	-0.3926
	deviation	0.148	0.4069	0.6812	0.69351
	Erturk et al.	-0.1951	-0.4272	-0.4491	-0.4469
0.06	present	-0.19539	-0.42961	-0.45247	-0.44875
	deviation	0.1507	0.5648	0.7504	0.41419
	Erturk et al.	-0.1392	-0.348	-0.398	-0.4259
0.04	present	-0.13948	-0.3502	-0.40161	-0.42999
	deviation	0.199	0.6313	0.9068	0.95915
	Erturk et al.	-0.0757	-0.2223	-0.2633	-0.2907
0.02	present	-0.07586	-0.22359	-0.26544	-0.29683
	deviation	0.2061	0.5785	0.8109	2.10802

Table 5 Percentage difference of centerline *v*-velocity with Erturk, Corke & Gokcol (2005).

x	Re	1000	5000	7500	10000
	Erturk et al.	-0.0973	-0.2441	-0.2991	-0.3419
0.985	present	-0.09734	-0.2447	-0.3002	-0.34336
	deviation	0.03864	0.2478	0.3701	0.42732
	Erturk et al.	-0.34	-0.57	-0.5434	-0.5124
0.955	present	-0.34037	-0.572	-0.5465	-0.51579
	deviation	0.10971	0.3542	0.5751	0.66101
	Erturk et al.	-0.5263	-0.4318	-0.4283	-0.4256
0.91	present	-0.5266	-0.4338	-0.4316	-0.42983
	deviation	0.05605	0.4662	0.7675	0.99295
	Erturk et al.	-0.5132	-0.4147	-0.4118	-0.4078
0.895	present	-0.5135	-0.4166	-0.415	-0.41212
	deviation	0.05787	0.4673	0.7722	1.05983
	Erturk et al.	-0.4407	-0.3806	-0.3755	-0.3715
0.865	present	-0.44094	-0.3824	-0.3784	-0.37568
	deviation	0.05378	0.4669	0.7782	1.12598
	Erturk et al.	-0.4028	-0.3624	-0.3574	-0.3538
0.85	present	-0.40304	-0.3641	-0.3602	-0.35787
	deviation	0.06008	0.4647	0.7865	1.1515
	Erturk et al.	0.0258	0.0117	0.0099	0.0088
0.5	present	0.02578	0.0116	0.0097	0.00861
	deviation	-0.0593	-0.641	-1.8865	-2.2075
	Erturk et al.	0.3756	0.3699	0.3616	0.3562
0.15	present	0.37599	0.3716	0.3643	0.35917
	deviation	0.10463	0.4526	0.7467	0.8338
	Erturk et al.	0.3605	0.407	0.395	0.3885
0.12	present	0.36091	0.4088	0.3979	0.39128
	deviation	0.11318	0.4484	0.743	0.71609
	Erturk et al.	0.346	0.426	0.4137	0.4056
0.105	present	0.34637	0.4279	0.4168	0.4082
	deviation	0.10723	0.4568	0.7503	0.64078
	Erturk et al.	0.3041	0.4426	0.4495	0.4449
0.075	present	0.30444	0.4452	0.4532	0.44772
	deviation	0.11213	0.5879	0.8162	0.63363
	Erturk et al.	0.2746	0.4258	0.4494	0.4566
0.06	present	0.27498	0.4286	0.4537	0.46091
	deviation	0.13875	0.648	0.9564	0.94415
	Erturk et al.	0.1792	0.3263	0.3608	0.3844
0.03	present	0.17946	0.3288	0.3651	0.39503
	deviation	0.1423	0.7665	1.2026	2.76587
	Erturk et al.	0.1019	0.216	0.2509	0.2756
0.015	present	0.10207	0.2178	0.2543	0.28308
	deviation	0.16683	0.8505	1.3475	2.7148

Table 6 Percentage difference of centreline *u*-velocity with Botella & Peyret (1998).

y	Botella & Peyret	Present	Deviation
	160×160	513×513	
0.9766	0.66442	0.66428	-0.0213
0.9688	0.58084	0.58069	-0.0251
0.9609	0.51693	0.51678	-0.029
0.9531	0.47233	0.47217	-0.0341
0.8516	0.33722	0.337	-0.0656
0.7344	0.18867	0.18856	-0.0634
0.6172	0.05707	0.05696	-0.1908
0.5	-0.06205	-0.06205	0
0.4531	-0.1082	-0.10817	-0.0258
0.2813	-0.28037	-0.28028	-0.0305
0.1719	-0.38857	-0.38829	-0.0723
0.1016	-0.30046	-0.30011	-0.1139
0.0703	-0.2229	-0.22262	-0.1249
0.0625	-0.20233	-0.20207	-0.128
0.0547	-0.18129	-0.18105	-0.1313

Table 7 Percentage difference of centreline *v*-velocity with Botella & Peyret (1998).

x	Botella & Peyret	Present	Deviation
	160×160	513×513	
0.9688	-0.22792	-0.22759	-0.14501
0.9609	-0.29369	-0.2933	-0.1331
0.9531	-0.35532	-0.35489	-0.12279
0.9453	-0.41038	-0.40991	-0.11414
0.9063	-0.52644	-0.52602	-0.08001
0.8594	-0.42645	-0.42631	-0.03435
0.8047	-0.32021	-0.32008	-0.04082
0.5	0.0258	0.02578	-0.05737
0.2344	0.32536	0.32519	-0.05293
0.2266	0.33399	0.33381	-0.05461
0.1563	0.37692	0.37665	-0.0724
0.0938	0.33304	0.33277	-0.08113
0.0781	0.30991	0.30965	-0.08348
0.0703	0.29627	0.29602	-0.08516
0.0625	0.28071	0.28046	-0.08749

Table 8 Percentage difference of centreline *u*-velocity with Bruneau & Saad (2006).

y	Bruneau & Saad 1024×1024	Present 513×513	Deviation
0.9688	0.5803	0.5807	0.0655
0.9531	0.4724	0.4722	-0.0461
0.7344	0.1886	0.1886	0
0.5	-0.06205	-0.06205	0
0.2813	-0.2804	-0.2802	-0.0414
0.1016	-0.30029	-0.3001	-0.3001
0.0625	-0.20227	-0.202	-0.0984

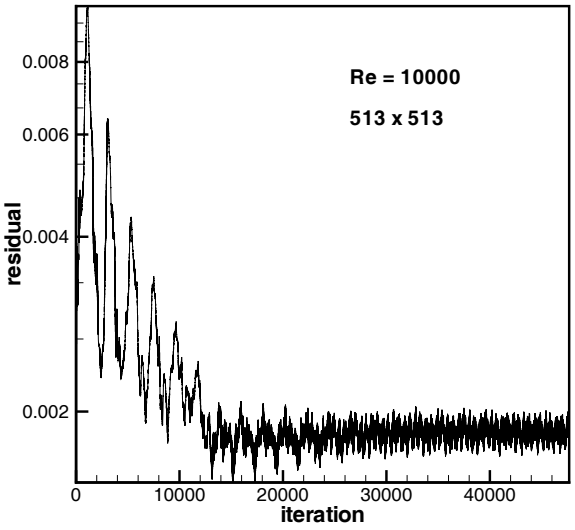

Fig. 11 Residuals on a 513×513 grid as a function of number of fine grid iterations for Re=10000.

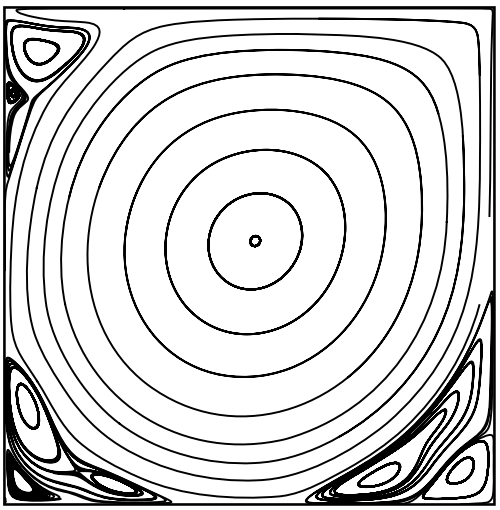

(a)

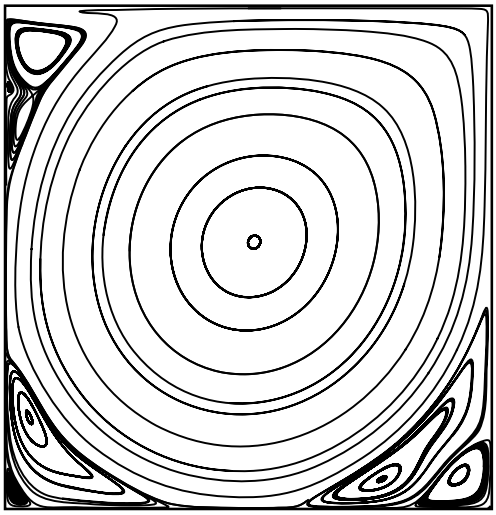

(b)

Fig. 12 Streamline contours for Re=10000. (a) No. of iterations=20000 (b) No. of iterations=42000.

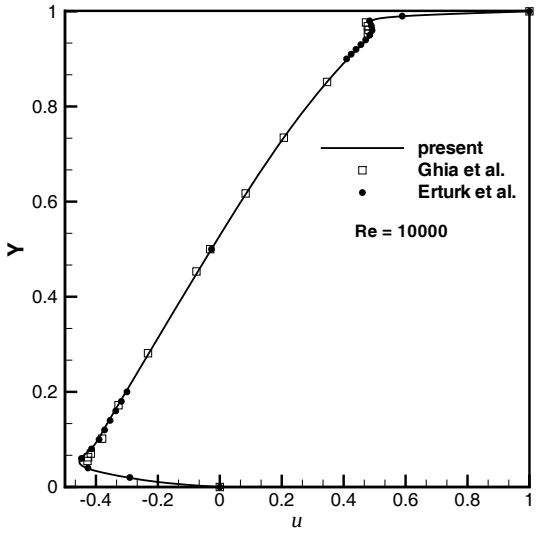

(a)

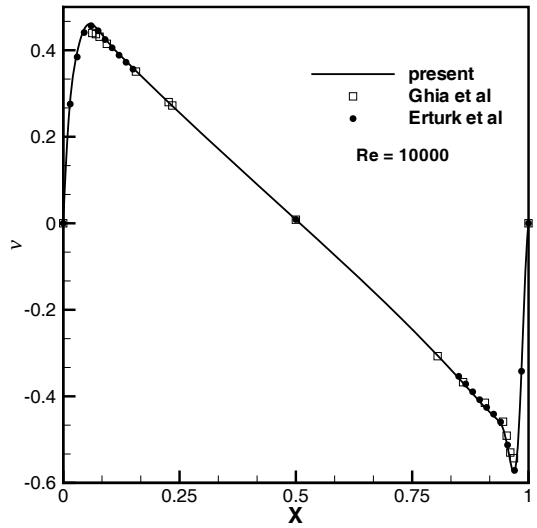

(b)

Fig. 13 Midplane velocity profiles passing through geometric centre for Re=10000.

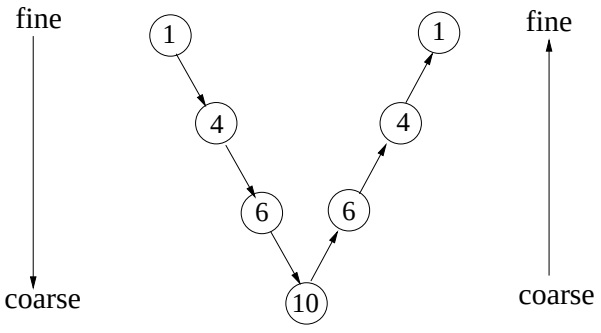

Fig. 14 V-cycle.

The performance of the multigrid method used for the present computations is described. Expectedly the multigrid full approximation scheme shows a faster convergence. All the results presented in

this paper were performed using the V-cycle (Fig. 14). Tests were conducted on both 2-level and 4-level V-cycles and increasing the level further did not pay additional dividend. The number of iterations performed at each grid level is shown inside the circles (Fig. 14). The computational effort is reported in terms of equivalent fine-grid sweeps that are usually referred to as work units. Fig. 15 presents the history of mass residual on a 129×129 grid as a function of the number of work units 1-, 2- and 4-level computations for various Reynolds numbers. The number of iteration required increases with increase in Reynolds number. A 4-level multigrid cycle shows better convergence than a 2-level multigrid cycle. Fig. 15 shows that in the single-grid the residuals fall faster at the beginning and slow down thereafter whereas in the multigrid method the residual falls at a more or less constant rate. Table 9 summarizes the main computational features of the test calculation for 129×129 grids. The computations are performed on a Pentium 4 Processor, 3.2 GHZ, 1 GB RAM based server. It can be seen that the speed-up factor between single grid and multigrid is almost 10. This shows the potential of multigrid technique for improving the convergence over single-grid method. However, it takes around 500 minutes with 100% CPU when run in 513×513 grids which seems to be computationally demanding. This can be reduced when a high performance computing machine is used.

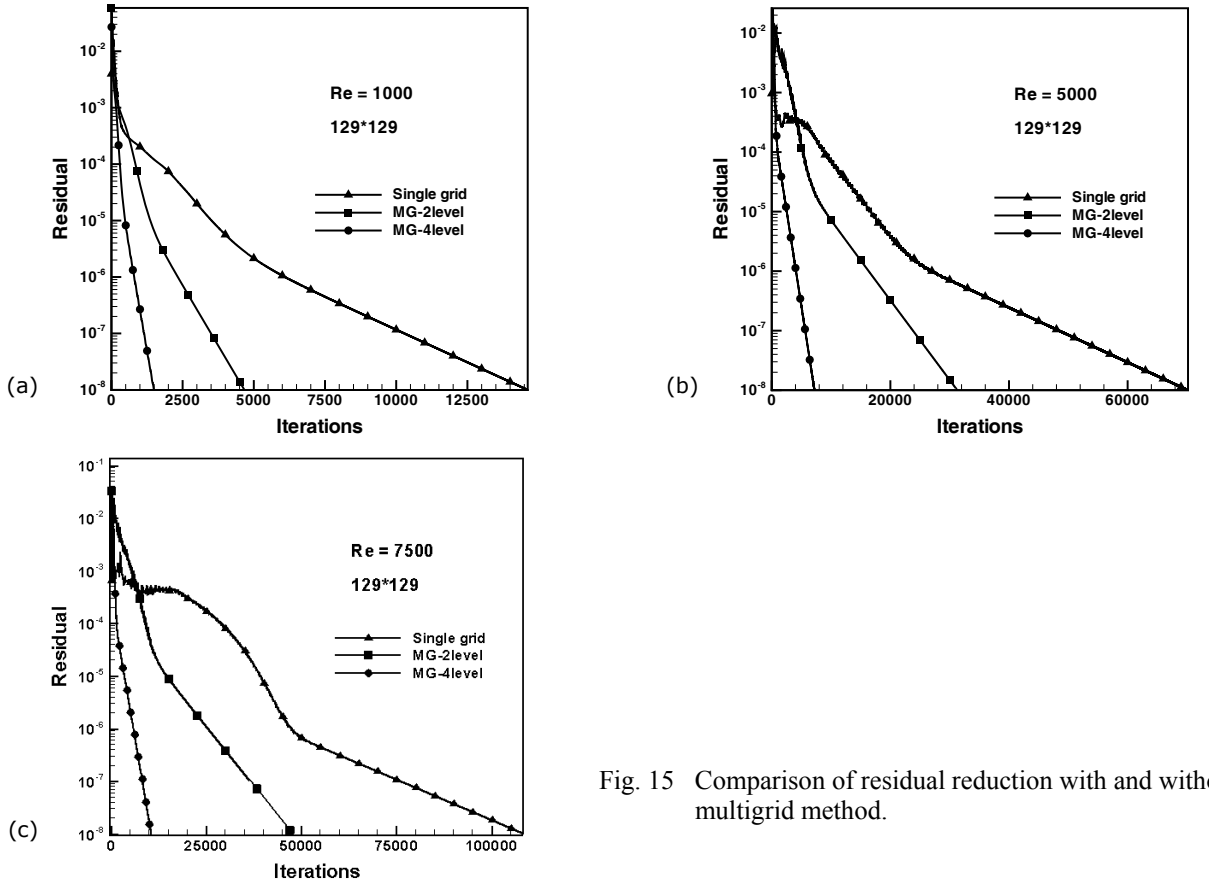

Fig. 15 Comparison of residual reduction with and without multigrid method.

Table 9 Computing times required by various versions of the solution method for 129×129 grids.

Reynolds number	Single grid (SG)	CPU time (minutes)		Speed-up MG/SG	
		MG-2 level	MG-4 level	MG-2 level	MG-4 level
1000	262	90	25	2.91	10.41
3200	644	225	81	2.86	7.95
5000	1048	445	130	2.35	8.06
7500	1425	513	158	2.77	9.01

6. CONCLUSIONS

Fine mesh solutions have been obtained very efficiently using the full approximation scheme multigrid method. The solutions computed in this work exhibit a very good representation of secondary and tertiary vortices for $\mathrm{Re} \leq 7500$, for which the solutions are stable and become unstable for the steady model with $\mathrm{Re} = 10000$ on the fine grid of 513×513 when small eddies are developed along the walls in the corner. The main conclusion drawn is that it is possible to obtain solutions with higher order discretization on a very fine grid by using multigrid technique. The results are compared with the accurate results available in the literature. It is found that the computed results in this work have a maximum of 1% deviation from those of Erturk, Corke and Gokcol (2005) and 0.19 % of Botella and Peyret (1998). This verification gives confidence in applying the method to other complex systems. The solutions presented here are very accurate and were found to agree well with the published results.

NOMENCLATURE

A	discrete equation coefficients
a	cell face area
p	dimensionless pressure
Re	Reynolds number
S	source term
R	residual
I	restriction and prolongation operator

Greek sysmbols

λ	under-relaxation parameter
ν	iteration number
Γ	diffusion coefficient
Φ	general property to be calculated
δ	correction

Superscripts

h	fine grid level
H	coarse grid level
u	u-momentum equation
v	v-momentum equation
´	fine grid corrections
´´	coarse grid corrections

Subscripts

i , j	node location in x and y directions
P,E,W,N,S	control volume grid points
nb	neighbour grid point
e,n,s,w	control volume faces
h	fine grid level
H	coarse grid level

REFERENCES

1. Auteri F, Parolini N, Quartapelle L (2002). Numerical investigation on the stability of singular driven cavity flow. *Journal of Computational Physics* 183(1):1–25.
2. Botella O, Peyret D (1998). Benchmark spectral results on the lid driven cavity flow. *Computers and Fluids* 27:421–433.
3. Bruneau C, Jouron C (1990). An efficient scheme for solving steady incompressible Navier-Stokes equations. *Journal of Computational Physics* 89(2):389–413.
4. Bruneau C, Saad M (2006). The 2d lid-driven cavity problem revisited. *Computers and Fluids* 35(3):326–348.
5. Cornelius C, Volgmann W, Stoff H (1999). Calculation of three dimensional turbulent flow with a finite volume multigrid method. *International Journal for Numerical Methods in Fluids* 31:703–720.
6. Doormaal JPV, Raithby GD (1984). Enhancements of the SIMPLE method for predicting incompressible fluid flows. *Numerical Heat Transfer* 7:147–163.
7. Erturk E, Corke T, Gokcol C (2005). Numerical solutions of 2-d steady incompressible driven cavity flow at high Reynolds numbers. *International Journal for Numerical Methods in Fluids* 48:74–774.
8. Fortin A, Jardak M, Gervais J, Pierre R (1997). Localization of Hopf bifurcations in fluid flow problems. *International Journal for Numerical Methods in Fluids* 24:1185–1210.
9. Ghia U, Ghia KN, Shin CT (1982). High-Re solutions for incompressible flows using the Navier-Stokes equations and a multi-grid method. *Journal of Computational Physics* 48:387–411.
10. Hayase T, Humphrey J, Greif R (1992). A consistently formulated quick scheme for fast and stable convergence using finite-volume iterative calculation procedures. *Journal of Computational Physics* 98:108–118.
11. Hortmann M, Peric M (1990). Finite volume multigrid prediction of laminar

natural convection: Bench-mark solutions. *International Journal for Numerical Methods in Fluids* 11:189–207.
12. Hou S, Zou Q, Chen S, Doolen G, Cogley AC (1995). Simulation of cavity flow by the lattice Boltzmann method. *Journal of Computational Physics* 118(2):329–347.
13. Karki KC, Sathyamurthy PS, Patankar SV (1996). Performance of a multigrid method with an improved discretization scheme for three-dimensional fluid flow calculations. *Numerical Heat Transfer* 29:275–288.
14. Leonard B (1979). A stable and accurate convective modeling procedure based on quadratic upstream interpolation. *Computational Methods in Applied Mechanics and Engineering* 19:59–98.
15. Lien F, Leschziner M (1994). Multigrid acceleration for recirculating laminar and turbulent flows computed with a non-orthogonal colocated finite volume scheme. *Computational Methods in Applied Mechanics and Engineering* 118:351–371.
16. Lilek Z, Muzaferija S, Peric M (1997). Efficiency and accuracy aspects of a full-multigrid SIMPLE algorithm for three-dimensional flows. *Numerical Heat Transfer* 31:23–42.
17. Peng Y, Shiau Y, Hwang R (2003). Transition in a 2-d lid-driven cavity flow. *Computers and Fluids* 32:337–352.
18. Peric M, Kessler R, Scheuerer G (1998). Comparison of finite volume numerical methods with staggered and colocated grids. *Computers and Fluids* 16:389–403.
19. Poliashenko M, Aidun C (1995). A direct method for computation of simple bifurcations. *Journal of Computational Physics* 121:246–260.
20. Rhie CM, Chow WL (1983). A numerical study of the turbulent flow past an isolated airfoil with trailing edge separation. *AIAA* 21:1525–1532.
21. Sathyamurthy P, Patankar S (1994). Block-correction based multigrid method for fluid flow problems. *Numerical Heat Transfer* 25(4):375–394.
22. Sivaloganathan S, Shaw G (1988). A multigrid method for recirculating flows. *International Journal for Numerical Methods in Fluids* 8:417–440.